AIAA 2001-0457

Shakedown of the Purdue Mach-6 Quiet-Flow Ludwieg Tube

S. P. Schneider, S. J. Rufer, L. Randall, and C. Skoch
Purdue University
West Lafayette, IN 47907-1282

39th Aerospace Sciences Meeting & Exhibit
8–11 January 2001
Reno, Nevada

Shakedown of the Purdue Mach-6 Quiet-Flow Ludwieg Tube

Steven P. Schneider*, Shann J. Rufer†, Laura Randall‡, and Craig Skoch§
School of Aeronautics and Astronautics
Purdue University
West Lafayette, IN 47907-1282

Abstract

Purdue University continues to develop a 9.5-inch Mach-6 Ludwieg tube for quiet-flow operation to high Reynolds number. The aerodynamic and mechanical design were reported earlier, along with the design and testing of several facility subsystems. Measurements of the coordinates of the completed upstream nozzle sections are here reported. The development and further testing of other facility systems are also described: these include the second round of burst-diaphragm tests, the bleed-slot suction system, and the driver-tube and contraction heating systems. Delivery of the quiet-flow nozzle is presently scheduled for February 2001. Progress in developing repeatable hot-wire calibrations is also reported.

Introduction

Hypersonic Laminar-Turbulent Transition

Laminar-turbulent transition in hypersonic boundary layers is important for prediction and control of heat transfer, skin friction, and other boundary layer properties. However, the mechanisms leading to transition are still poorly understood, even in low-noise environments. Applications hindered by this lack of understanding include reusable launch vehicles such as the X-33 [1], high-speed interceptor missiles [2], hypersonic cruise vehicles [3], and ballistic reentry vehicles [4].

Many transition experiments have been carried out in conventional ground-testing facilities over the past 50 years. However, these experiments are contaminated by the high levels of noise that radiate from the turbulent boundary layers normally present on the wind tunnel walls [5]. These noise levels, typically 0.5-1% of the mean, are an order of magnitude larger than those observed in flight [6, 7]. These high noise levels can cause transition to occur an order of magnitude earlier than in flight [5, 7]. In addition, the mechanisms of transition operational in small-disturbance environments can be changed or bypassed altogether in high-noise environments; these changes in the mechanisms change the parametric trends in transition [6].

For example, linear instability theory suggests that the transition Reynolds number on a 5 degree half-angle cone should be 0.7 of that on a flat plate, but noisy tunnel data showed that the cone transition Reynolds number was about twice the flat plate result. Only when quiet tunnel results were obtained was the theory verified [8]. This is critical, since design usually involves consideration of the trend in transition when a parameter is varied. Clearly, transition measurements in conventional ground-test facilities are generally not reliable predictors of flight performance.

Development of Quiet-Flow Wind Tunnels

Only in the last two decades have low-noise supersonic wind tunnels been developed [5, 9]. This development has been difficult, since the test-section wall boundary-layers must be kept laminar in order to avoid high levels of eddy-Mach-wave acoustic radiation from the normally-present turbulent boundary layers. A Mach 3.5 tunnel was the first to be successfully developed at NASA Langley [10]. Langley then developed a Mach 6 quiet nozzle, which was used as a starting point for the new Purdue nozzle [11]. Unfortunately, this nozzle was removed from service due to a space conflict. Langley also attempted to develop a Mach 8 quiet tunnel [9]; however, the high temperatures required to reach

*Associate Professor. Associate Fellow, AIAA.
†Research Assistant. Student Member, AIAA.
‡Ph.D. Candidate. Student Member, AIAA.
§Research Assistant. Student Member, AIAA.

Mach 8 made this a very difficult and expensive effort. The effort was in the end unsuccessful, and the Mach-8 tunnel has now been closed (Steve Wilkinson, private communication, November 2000). The new Purdue Mach-6 quiet flow Ludwieg tube may be the only operational hypersonic quiet tunnel in the world.

Background of the Purdue Mach-6 Quiet-Flow Ludwieg Tube

A Mach-4 Ludwieg tube was constructed at Purdue in 1992, using a 4-inch nozzle of conventional design that was obtained surplus from NASA Langley. By early 1994, quiet-flow operation was demonstrated at the low Reynolds number of about 400,000 [12]. Since then, this facility has been used for development of instrumentation and for measurements of instability waves under quiet-flow conditions (e.g., Ref. [13, 14, 15]). However, the low quiet Reynolds number imposes severe limitations; for example, the growth of instability waves under controlled conditions on a cone at angle of attack was only about a factor of 2 [16]. This is far smaller than the factor of $e^9 - e^{11}$ typically observed prior to transition, and small enough to make quantitative comparisons to computations very difficult.

A facility that remains quiet to higher Reynolds numbers was therefore needed. The low operating costs of the Mach-4 tunnel had to be maintained. However, hypersonic operation was needed in order to provide experiments relevant to the hypersonic transition problems described above. Operation at Mach 6 was selected, since this is high enough for the hypersonic 2nd-mode instability to be dominant under cold-wall conditions, and high enough to observe hypersonic roughness-insensitivity effects, yet low enough that the required stagnation temperatures do not add dramatically to the cost and difficulty of operation. Reference [17] describes the overall design of the facility, and the detailed aerodynamic design of the quiet-flow nozzle, carried out using the e^N method (see also Ref. [18]).

Attached flow should be maintained in the contraction of the nozzle, since the separation bubbles sometimes observed in wind tunnel contractions are generally unsteady, and would transmit noise downstream into the Mach-6 nozzle. Preliminary analyses have suggested that the low-frequency fluctuations present in the Langley Mach-6 quiet nozzle [11] may be caused by such a separation. Therefore, a detailed aerodynamic design of the contraction was also carried out [19]. Reference [19] also supplies a preliminary report on the detailed mechanical design of the nozzle and contraction, which was carried out during 1997-98. This mechanical design is not trivial, since quiet uniform flow requires very tight tolerances on surface contour and finish.

After some initial tests of fabrication procedures, a purchase order for fabrication of the nozzle and contraction was awarded in January 1999, to Dynamic Engineering Inc. (DEI), of Newport News, Virginia. Reference [20] reported on design and testing of some of the component parts, including the driver-tube heating, the as-measured contraction contour, and the throat-region mandrel fabrication and polishing experience. Ref. [20] also reports the results of numerous measurements of the surface roughness of the mandrel and various test pieces. Finally, Ref. [20] reports temperature measurements carried out on the heated driver tube. Ref. [21] reports on the design and fabrication of the support structure, diffuser, and second-throat section (which also serves as the sting support). It also reports experience with final contraction fabrication, and with operation of the vacuum system. Finally, Ref. [21] reports the contour measurements on the third attempt at throat-mandrel fabrication.

Delivery of the nozzle is currently scheduled for February 2001. This paper reports on additional shakedown details not described in Refs. [19], [20], and [21]. These details include the burst diaphragm apparatus, the contour measurements on nozzle sections 4 and 5, experience with the throat electroform, the bleed-slot suction plumbing, the heating apparatus for the contraction, the computed temperature distribution in the nozzle, and a new prediction of quiet-flow performance using this computed temperature distribution. The contour measurements for the remaining nozzle sections (6-8) are to be reported, along with initial tunnel performance measurements, in Ref. [22].

The Purdue Mach-6 Quiet-Flow Ludwieg Tube

Quiet facilities require low levels of noise in the inviscid flow entering the nozzle through the throat, and laminar boundary layers on the nozzle walls. These features make the noise level in quiet facilities an order of magnitude lower than in conventional facilities. To reach these low noise levels, conventional blow-down facilities must be extensively modified. Requirements include a 1 micron particle filter, a highly polished nozzle with bleed slots for the contraction-wall boundary layer, and a large settling chamber with screens and sintered-mesh plates for noise-reduction [5]. To reach these low noise levels in an affordable way, the Purdue facility has been

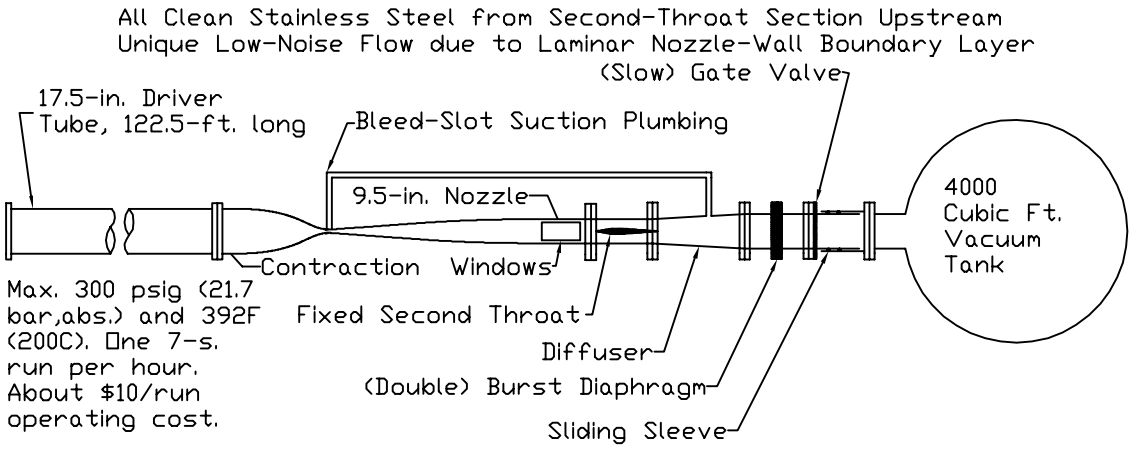

Figure 1: Schematic of Purdue Mach-6 Quiet-Flow Ludwieg Tube

designed as a Ludwieg tube [12]. A Ludwieg tube is a long pipe with a converging-diverging nozzle on the end, from which flow exits into the nozzle, test section, and second throat (Figure 1). A diaphragm is placed downstream of the test section. When the diaphragm bursts, an expansion wave travels upstream through the test section into the driver tube. Since the flow remains quiet after the wave reflects from the contraction, sufficient vacuum can extend the useful runtime to many cycles of expansion-wave reflection, during which the pressure drops quasi-statically.

Figure 2 shows the nozzle of the new facility. The region of useful quiet flow lies between the characteristics marking the onset of uniform flow, and the characteristics marking the upstream boundary of acoustic radiation from the onset of turbulence in the nozzle-wall boundary layer. A 7.5-deg. sharp cone is also drawn on the figure. The cone is drawn at the largest size for which it is likely to start [23, 24].

Contraction Heating

The driver tube has been carefully cleaned, and a heating system has been installed on the contraction. The contraction must be heated, since the gas for the first second of the 7-s. run will originate in the contraction. Since the nozzle is unheated and uninsulated, to keep it cooler, it will serve as a heat sink. Heat must be injected at the contraction to overcome this heat sink, while maintaining uniformity of the driver-tube temperature.

An off-the-shelf commercial heating system has been procured for this contraction heating. Three 3000W commercial band heaters are installed on the contraction. A fourth 400W heater is installed on the bleed-lip ring to allow heating the nozzle throat above the stagnation temperature. These are controlled from a set of four zero-switching commercial heater controllers (TEMPCO Electric Heater Co., AIM type). Negligible electromagnetic interference has been verified in a preliminary test. The four heaters can be controlled by panel settings. They can also be computer-controlled through a serial connection.

The system has been installed and tested, with a blind flange taking the place of the nozzle. Thermocouples are used to monitor the outside contraction temperature. No thermocouples are installed on the inside of the contraction, so as not to risk introducing disturbances into the flow. The driver tube can be successfully heated to $180°C$, as reported earlier in Ref. [20]. The upstream end of the contraction is also readily heated to $180°C$, without covering the complex assembly with any insulation. However, the downstream end only reaches $160°C$ when no insulation is used. Since operation at a stagnation temperature of 380K or $110°C$ is currently planned, following Ref. [23], no difficulties are presently expected. The actual stagnation temperature of the driver-tube gas will be measured in operation using cold-wire techniques.

The geometry of the nozzle is far too complex to solve analytically for the temperature distribution, without oversimplifying the problem. The solution was carried out using finite element analysis. The program used to solve the equations for heat conduction in a solid was FEHT (Finite Element Heat Transfer) written by F-Chart Software. The nozzle was approximated using an axisymmetric geometry.

The nozzle was modeled out to the end of section

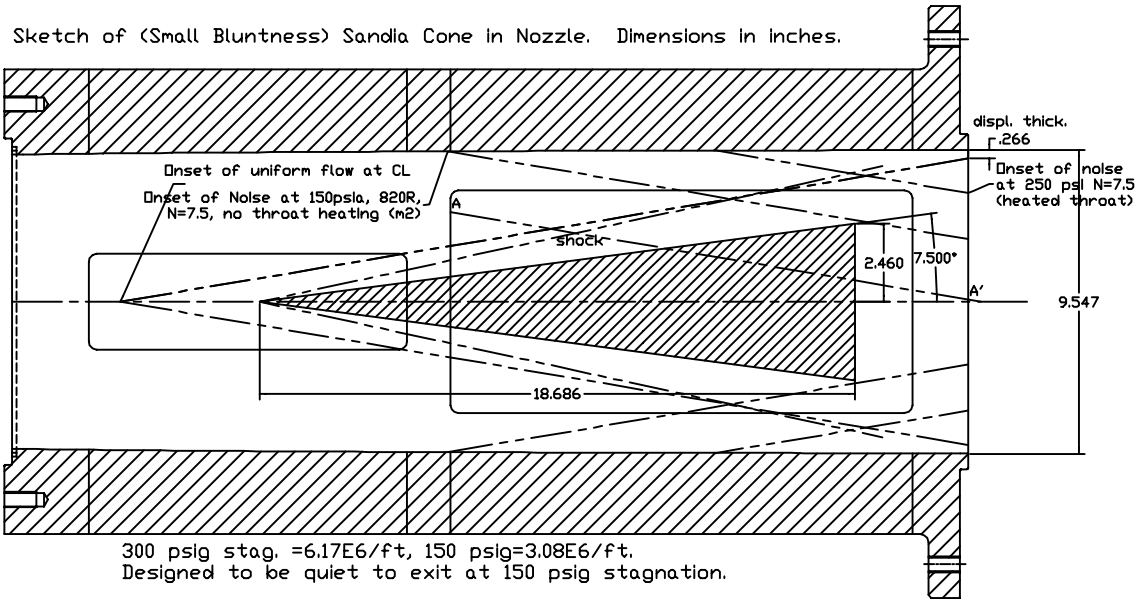

Figure 2: Schematic of Mach-6 Quiet Nozzle with Model

4, or about halfway to the end of the nozzle. Since the results showed that the temperature decreases to near ambient by the end of this section, it was not necessary to model the remainder. Fig. 3 shows the geometry, along with contours of the temperature distribution. The high spots are flanges, where the sections are joined together.

The types of boundary conditions that FEHT allows are a set temperature, a heat flux, or convective heating or cooling. On the inside surface, where the air is, the boundary condition was set to adiabatic, or zero heat flux, since the inside air should reach approximate equilibrium. The left side was set to the temperature that the contraction band heaters will maintain. The right wall, where the nozzle continues downstream, was set to adiabatic or ambient temperature, forming two different cases. The outside wall was set to convective cooling. This requires specifying an ambient air temperature, which was chosen as $25°C$, and a convective heat transfer coefficient. It should be noted that radiative heat transfer is not accounted for in FEHT, so the actual temperatures may be lower than computed here.

The convective heat transfer coefficient is found by using an empirical correlation for external free convection on a long cylinder [25]. As a first approximation a constant coefficient was assumed, using a surface temperature halfway between the contraction temperature and the ambient temperature. Once a solution was found using this method, the heat transfer coefficient was allowed to vary based on both changes in outer diameter and on the temperature distribution from the first approximation.

Comparisons of the adiabatic-end case and the ambient-end case are necessary to determine whether a sufficient length of the nozzle was modeled. Figure 3 shows contour plots of the nozzle with a $160°C$ driver tube and both adiabatic and ambient-temperature ends. These results were calculated using the constant-convection heat transfer coefficient mentioned earlier. It can be seen in Fig. 3 that there is very little difference between the two plots except for the $30°C$ contour, which is shifted slightly.

Figure 4 shows the temperature distributions on the inside of the nozzle for the $160°C$ driver-tube case, using both the constant and variable heat transfer coefficients. The ambient-end cases separate slightly, but become closer together at the end due to the ambient-end boundary condition. The adiabatic-end varying-coefficient case results in a downstream end that is slightly higher, at $32.5°C$, compared to the constant coefficient case, at $29.5°C$. However, the end temperature is still close to the ambient temperature of $25°C$. This shows that the length of the nozzle that has been modeled is sufficient to show most of the temperature drop to ambient, and that this happens long before the end of the 2.6-m nozzle. It would be possible to model a larger portion of the nozzle, but FEHT has a limit in the number of elements it can process, so a larger model would require a less refined solution. It seems

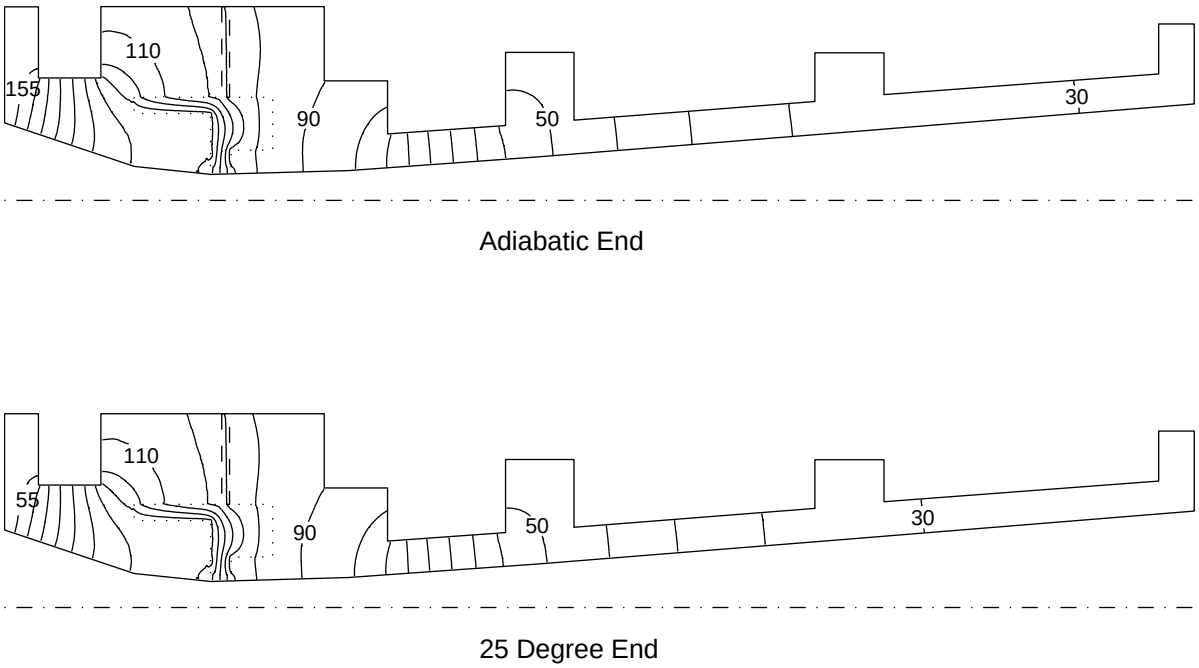

Figure 3: Contours of the Temperature Distribution in the Nozzle, in Celsius

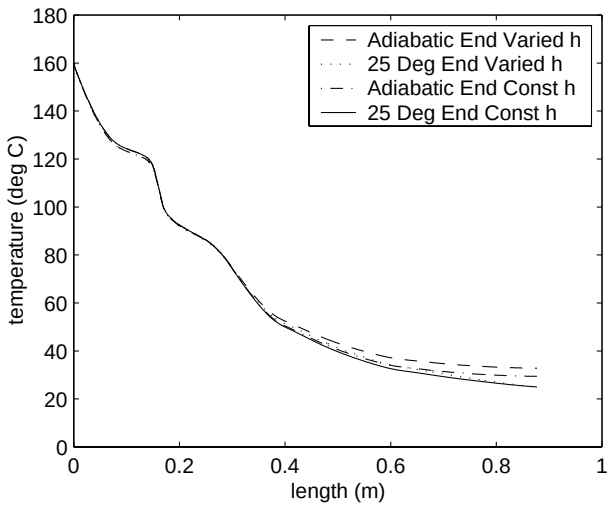

Figure 4: Inside-Surface Temperature Distribution Computed in the Nozzle

that the discrepancy is small enough that this solution is sufficiently accurate. Once the tunnel is completed, the computation will be verified by using an arrangement of external thermocouples along the nozzle.

Quiet-Flow Predictions Based on Computed Inside Surface Temperatures

The computed wall temperature distribution was used to recompute the instability of the boundary layer on the nozzle wall, to obtain an improved prediction of the quiet-flow performance. The methods described in Refs. [17] and [18] were used; they consist of a method-of-characteristics inviscid solution, a finite-difference boundary-layer computation, and a parallel-flow linear instability analysis.

The temperature distribution was taken from the $160°C$ stagnation-temperature case, using the computation for the adiabatic downstream end, for constant heat-transfer coefficient. A stagnation pressure of 150 psia was used, together with a stagnation temperature of $160°C$. The computation started at the bleed lip, just upstream of the throat. Although these throat details were not modeled in the FEHT computation, the FEHT results were simply taken as the nozzle-wall temperature. This seemed like a reasonable approximation for the case of an unheated throat. The wall-normal boundary-layer grid contained 201 points, and 687 streamwise stations were used. As in the earlier work, the first-mode, second-mode, and Görtler instabilies

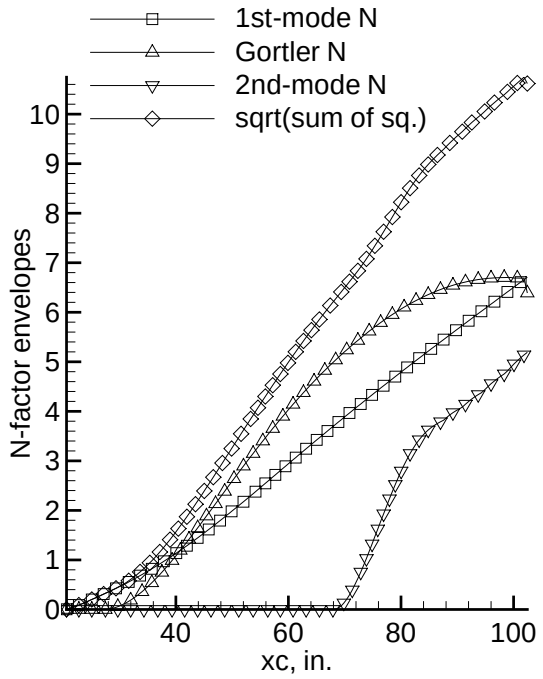

Figure 5: Nozzle-Wall N-factor Envelopes Using Computed Wall Temperatures

were computed. The overall effect was estimated by a combined N factor made up of the square root of the sum of the squares of the three component N factors; transition was assumed to occur when this total N factor was 7.5 [17, 18].

The envelope of the individual N factor curves are shown together with the total N factor in Fig. 5. The first-mode instability reaches larger amplitudes than in earlier computations, where the nozzle-wall temperature was assumed to drop linearly between the throat and the exit (cp. Fig. 14 of Ref. [18]). The second-mode instability also reaches larger amplitudes, although the Görtler instability changes little. This seems generally consistent with the earlier results. The first and second-mode waves grow more rapidly, apparently because the nozzle wall temperature is lower near the throat, and drops more rapidly away from the throat. The Reynolds number based on the overall length of the quiet-flow region drops from 10.2 million (case m2 of Ref. [18]) or 8.1 million (case m3) to 7.6 million (present case).

The onset of noise is predicted to lie along the line marked `A-A'` in Fig. 2. It is apparent from Fig. 2 that the noise would impinge on the aft end of a large slender cone, at these tunnel conditions. However, many assumptions must be made to obtain these estimates of transition on the nozzle wall. If the onset of noise is actually experienced during tunnel operation near the line `A-A'`, the nozzle-wall temperature distribution will have to be modified through bleed-lip heating, the addition of insulation on the contraction or nozzle, or additional band heaters placed on the upstream end of the nozzle.

Nozzle Contour Measurements

Background

The accuracy and waviness of the nozzle contour is critical for mean flow uniformity and laminar flow control, as discussed in detail in Ref. [20]. In addition to the references cited in Ref. [20], the author has also become aware of Ref. [26], describing measurements and computations related to flaws in the Mach 6.8 nozzle of the Göttingen Ludwieg tube. In this nozzle, the measured pitot pressure varied by roughly 4% near the centerline, in some regions. Detailed measurements of the nozzle contour were obtained, and the pitot-pressure variations were reproduced with good accuracy by a high-resolution computation. Although the nozzle contour contains wavy regions with an amplitude of about 0.2 mm and a slope of roughly 0.04 mm/mm, the pitot variations remained even when these wavy regions were removed from the simulated contour. It is thought that the pitot variations are due to errors that remain even in the smoothed contour. The design method used to determine the original contour for this 30-year old nozzle is not described, nor are the deviations between the design contour and the as-measured contour.

Contour measurements of the mandrel for the throat-region electroform are reported in Ref. [21]. The throat-region electroform is enclosed in nozzle sleeve sections 1–3, and ends at tunnel station $z = 19.265$ in., where $z = 0$ at the nozzle throat.

Nozzle Section 4

Since the mandrel was ground to within about 0.0002 inches of the designed shape, and since the electroform is presumed to have a matching accuracy, DEI decided to cut the next section, nozzle section 4, about 0.001 inches oversize, and hand work the downstream end of the (softer) electroform to match it. Measurements were again obtained on 4 azimuthal rays, at 90-deg. intervals, although only on 0.100-inch spacings, rather than the usual 0.050-inch spacings, due to an oversight. Fig. 6 shows the measured contour and the deviation from nominal. Section 4 extends from $z = 19.265$ in. to $z = 30.265$

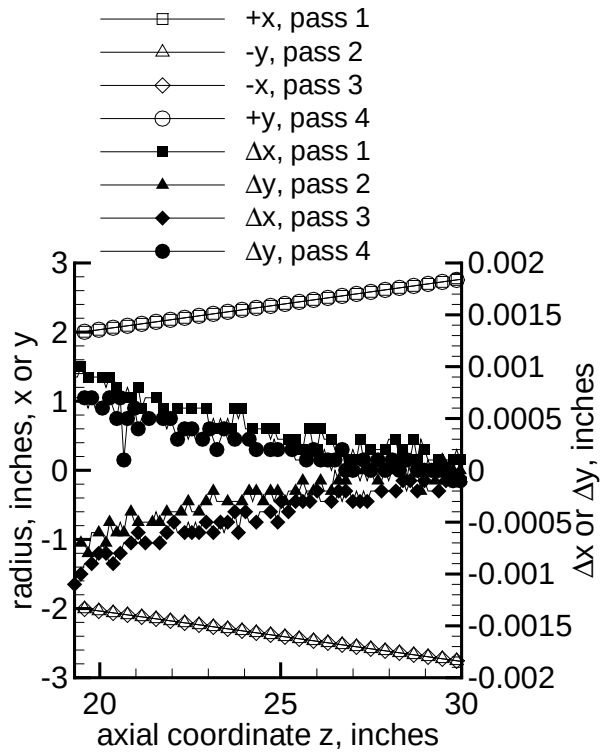

Figure 6: Contour Measurements for Nozzle Section 4

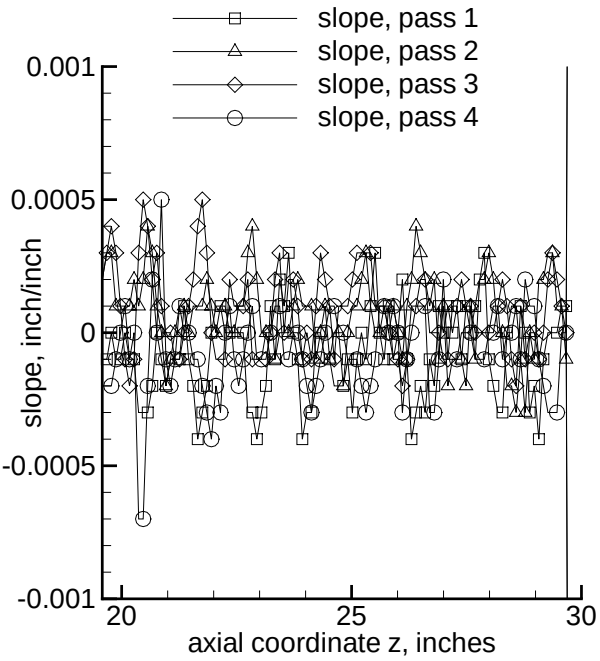

Figure 7: Contour Slope for Nozzle Section 4

in. The last downstream part of the section is not shown, since at the time of the measurement it contained only a cylindrical flat. This flat was later taken out when the end was recut after assembly to section 5 and realignment on the lathe.

Fig. 6 shows that the section is slightly more than 0.001 inches oversize at the upstream end, tapering to nearly the exact design size at the downstream end. Fig. 7 shows the slope, computed by fitting a straight line to 6 adjacent points (at 0.100 intervals). The slope remains well within the 0.001 inch/inch specification, except at the downstream end where it transitions into the flat. The section is within specification, except for the upstream end where it is slightly more than 0.001 inches oversize.

Nozzle Section 5

Measurements were then carried out on nozzle section 5, after it was assembled to section 4, realigned on the lathe, and very carefully cut. Section 5 extends from $z = 30.265$ to $z = 42.265$ in. Fig. 8 shows the measurements of the contour and the deviations, which extend upstream into section 4, past the overlap with the previously machined surface of section 4. Section 5 is about 0.0013 inches

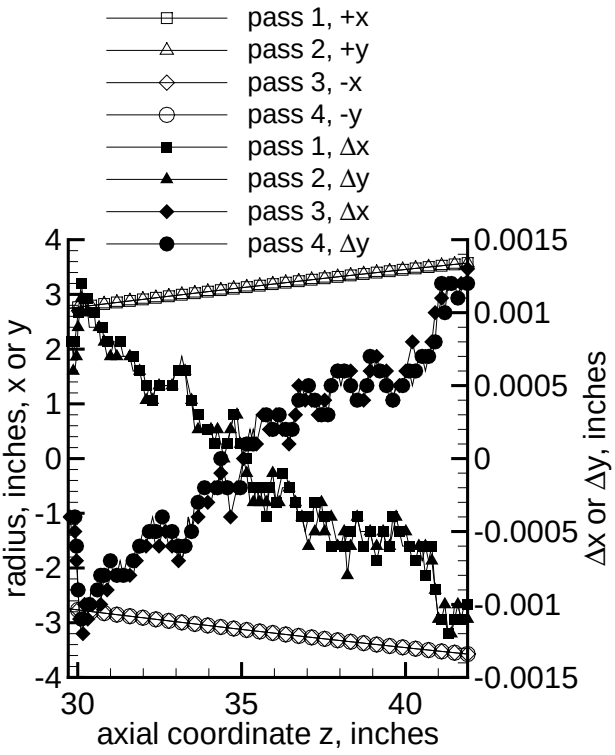

Figure 8: Contour Measurements for Nozzle Section 5

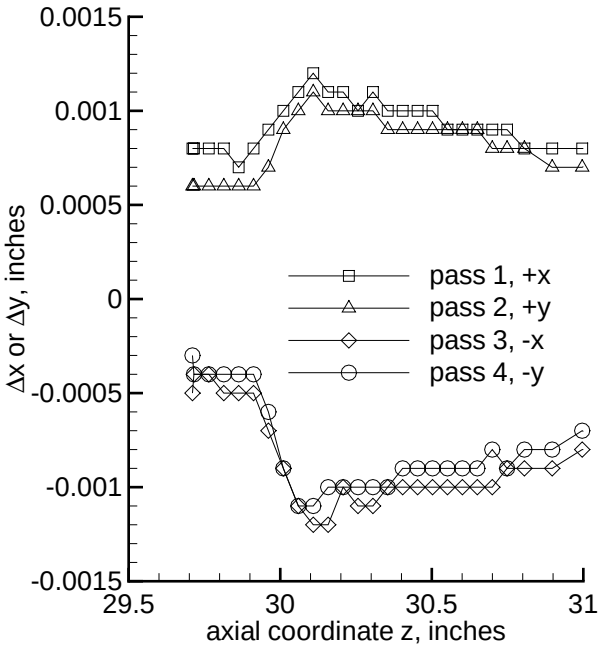

Figure 9: Detail of Section 5 Contour Near Joint

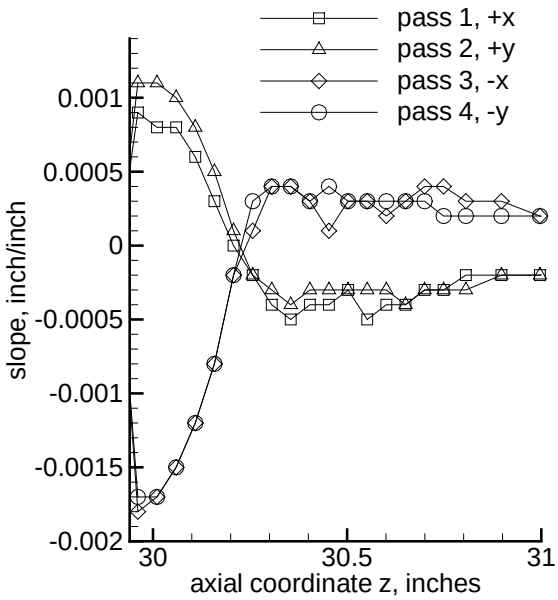

Figure 10: Detail of Section 5 Contour Slope Near Joint

oversize at the upstream end, and about 0.001 inches undersize at the downstream end. A wave is noticeable near $z = 30$ inches, near the joint between the first and second machinings of the end of section 4. Fig. 9 shows a detail of this area. The wave has an amplitude of slightly less than 0.001 inches, and is distributed over about 0.2 inches. This wave is the residual mismatch between the final cut on section 4 and the final cut on section 5, which overlap near the downstream end of section 4. Since a best-fit alignment with the ideal shape is carried out for each set of measurements before computing the deviations, the details may not agree precisely between measurements.

Near the joint, the measurements were obtained at 0.050-inch intervals. Following earlier work by Steve Wilkinson at NASA Langley, the local slope is computed by fitting a straight line to 11 points. This averages local slopes over a minimum of about 0.5 inches. Fig. 10 shows the results near the joint, which is the only place with slopes greater than 0.001 inch/inch. Near the machining overlap, the maximum magnitude is nearly 0.002 inch/inch (the 0.001 near-step averaged over 0.5 inches).

The acceptability of local waviness is being evaluated using a procedure developed after reviewing the literature [20]. The combination of local slope amplitude and the total size of the local flaw seems to be the critical factor in causing problems with mean-flow uniformity and early transition. Following computation of the local slope, therefore, regions were identified where the magnitude of the local slope exceeded 0.001 inch/inch. The total amplitude of the contour deviation was computed in these regions, by integrating the area under the slope curve. A variable `FLAW` was computed in these regions, as the product of the local maximum slope and the total amplitude of the slope deviation. The contract for nozzle fabrication provides incentive fees for maintaining `FLAW` below 1×10^{-6} inches. Near $z = 30$ in., the value of `FLAW` peaks below 0.5×10^{-6} in. Although the local slope reaches near 0.002 inch/inch, the region with slopes above 0.001 inch/inch extends over less than 0.2 inches of axial distance, during which the total change in contour deviation is about 0.0005 inches or less. The computed product is well within the specification.

Burst-Diaphragm Apparatus

Introduction

The burst-diaphragm apparatus is a critical part of the facility, because it must allow low-cost, rapid initiation of flow from accurately repeatable stagnation conditions. Any other fast-acting valve with the

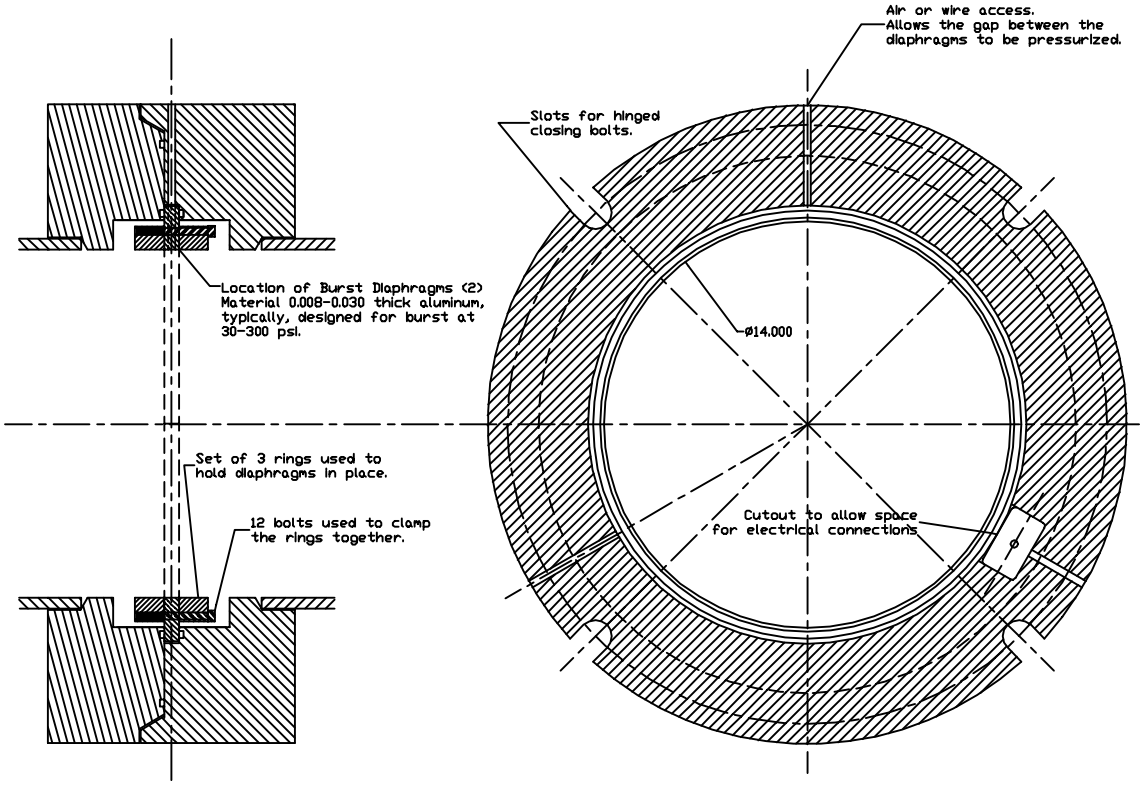

Figure 11: Schematic of Burst Diaphragm Apparatus

requisite 12-inch-diameter open area was thought to be too difficult and costly. The burst diaphragm apparatus is located downstream of the test section, so disturbances will not affect the quiet flow (Fig. 1). Fig. 11 shows a scaled drawing of the burst diaphragm assembly, along with the diaphragm-holder rings that are inserted into it. The assembly is a code-stamped pressure vessel rated for full tunnel pressure. It is designed to allow the use of a variety of different diaphragm holders, and a variety of access ports are provided.

For example, while the current diaphragm holders are designed for use of classic double-diaphragm methods, it is also possible to fabricate a holder that uses a single mylar diaphragm, broken electronically [13]. This may allow tunnel operation to stagnation pressures as low as about 1 atm., allowing studies of high-altitude viscous-interaction effects. A run time of 5 sec. at a total pressure of 1 atm. seems feasible, allowing unit Reynolds numbers roughly one half of those used successfully in Ref. [27].

Double-Diaphragm Tests

Classic double-diaphragm technique is presently being used. After the diaphragms have been securely placed in the tube, everything downstream of the diaphragms is placed under vacuum conditions while the upstream side is brought to the desired pressure. The space between the diaphragms is then bled down towards vacuum. When sufficient differential pressure is reached across the diaphragms they will burst, initiating flow. Repeatability of diaphragm burst pressure is tricky, and essential to successful operation. Tests of this system have therefore been ongoing since summer 1999; details are reported in Ref. [28].

The final diaphragm holder consists of a set of 3 rings held together by twelve 1/2-inch bolts, as shown in Fig. 12. The tool-steel rings are hardened after machining, so that in combination with the large bolts, it is possible to clamp the diaphragms tightly enough that they do not slip. A torque wrench is used to ensure repeatable clamping force. The ring faces must be flat, so that even clamping pressure is applied when the bolts are evenly torqued. The first-generation rings with twelve 1/4-inch bolts could not supply sufficient clamping pressure to preclude diaphragm slippage, without breakage of the grade 8 bolts. Although the first-generation rings included a dimpled mating sur-

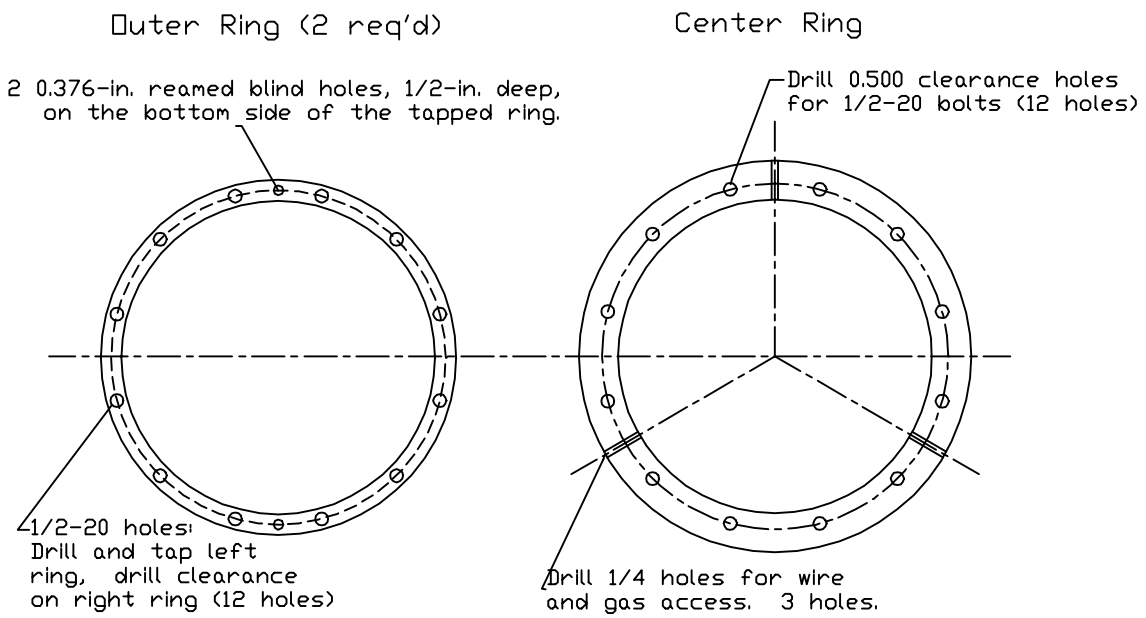

Figure 12: Schematic of Burst Diaphragm Rings

face to help hold the diaphragms in place, this was not found to be necessary. The two blind holes in the base of the assembly are used to hold it in place while the bolts are torqued.

The three diaphragm-holder rings have the same 12-inch inner diameter as the tunnel. The diaphragms have the same outer diameter as the smaller of the rings and also contain the same bolt pattern as the rings. The entire apparatus takes approximately 10 minutes to set up. Two sets of rings have been fabricated, so that one can be assembled while awaiting pump-down of the tunnel using the other.

Sealing between the rings and the diaphragms is also critical, and must be achieved with a minimum of complexity in order to speed tunnel operations. The final design uses diaphragms which are drilled for passage of the 1/2-inch bolts, so that diaphragm material is present on the outside of the bolts. When this is done, a sufficiently good metal-metal seal is achieved without the use of O-rings or other seals. This eases assembly operations, without making diaphragm fabrication too complex. A die may eventually be fabricated so that the diaphragms can be efficiently stamped out in large quantities. The estimated total cost is about $2-3 per diaphragm, in quantity.

Normally, the burst diaphragms break clean at the edge of the rings, around the full diameter, and blow downstream into the vacuum tank. Figure 1 shows a slow gate valve that is placed downstream of the burst-diaphragm apparatus. This allows raising the burst-diaphragm section to atmospheric pressure without repressurizing the vacuum tank, which saves compressed air. Although a butterfly valve was initially used here, due to the much lower cost, pieces of burst diaphragm would catch on the butterfly while being blown downstream, damaging the seal and causing operational problems. The full-port gate valve now used allows full clearance for the diaphragm fragments.

It was necessary to find diaphragm materials which break at the proper pressures to allow operation over the full range of desired stagnation pressures (approx. 20-140 psig). The cost and availability of the diaphragm material is also a major issue, particularly since suitable thicknesses tend to be near the thinnest of those that are commonly produced. Several different diaphragm materials have been tested (3003-H14, 5052-H32, 6061-O, and 6061-T6 series aluminum), along with several thicknesses (varying from 0.008 inches to 0.032 inches).

Once the rings and diaphragms have been assembled, they are placed inside the tube. During a run, the upstream and gap pressures are increased simultaneously, though the gap pressure is brought up at a much slower rate than the upstream pressure. Once the desired upstream pressure has been reached, the air in the gap is slowly bled to vacuum, until sufficient differential pressure is obtained, at which point the diaphragms burst. The differential pressure needs to be carefully monitored on both the

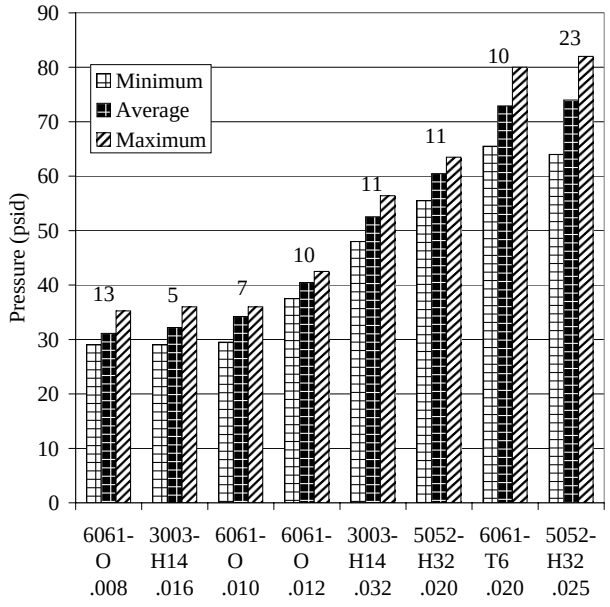

Figure 13: Variation in Break Pressures of Burst Diaphragms

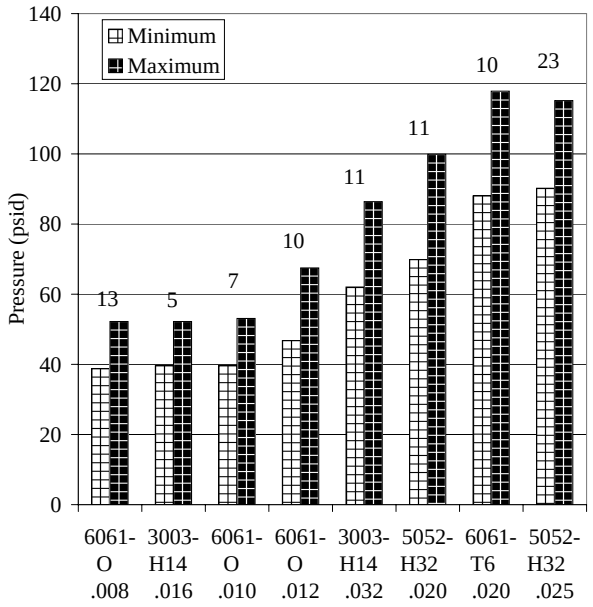

Figure 14: Workable Driver-Pressure Ranges

upstream and downstream diaphragms, to ensure that the diaphragms do not burst prematurely, and so that the downstream diaphragm does not break prior to the upstream diaphragm.

The differential pressure, at the time of the burst, was calculated across both the upstream and downstream diaphragm. It was assumed that the diaphragm which saw the largest differential pressure was the one that actually broke first. Fig. 13 shows this variation in burst pressure for each material type and thickness. The plot shows the minimum, maximum, and average burst pressures measured during all of the runs that were carried out for each material. The number of runs carried out for each case is shown above the bars. Ideally, the maximum and minimum pressures would be equal. However, the inevitable scatter reduces the range of workable driver pressures.

Since in the ideal case the gap pressure can be set to exactly half of the upstream driver pressure P_{up}, the condition that the diaphragms not break during set up requires that

$$0.9P_{break,minimum} > 0.5P_{up}, \qquad (1)$$

where $P_{break,minimum}$ is the minimum in the variation of the break pressure of the diaphragm, and the factor 0.9 gives a 10% margin. To initiate flow, gap pressure is bled down toward the downstream pressure, so the differential pressure across the upstream diaphragm approaches the upstream pressure. To ensure that the diaphragms break in this case, the upper limit of the break pressure is given by

$$1.1P_{break,maximum} < P_{up}, \qquad (2)$$

where $P_{break,maximum}$ is the maximum in the variation of the break pressure of the diaphragm, and the factor 1.1 gives the same 10% margin. Both these equations take into account that the downstream end of the tunnel is at a relatively high vacuum.

Using the variation in observed break pressure, the upper and lower limits of workable driver pressure are found using these equations. Improved repeatability results in an increased range of upstream working pressures. The results are plotted in Fig. 14. A good range of working pressures has been identified.

The lowest pressure differential across the diaphragms was used to determine this maximum workable driver pressure. However, during only a few of the tests was the differential burst pressure this low. For example, during most of the tests the differential burst pressure for the 5052-H32 was greater than 73 psid, although the minimum shown was 64 psid. Because of this, the maximum driver pressure shown in Figure 14 is much less than that which can actually be achieved. For example, during actual proof testing of the double-diaphragm setup, the 5052-H32 material allowed a maximum driver pressure of 150 psia.

The final materials and thicknesses to be used for the diaphragms have been chosen according to the pressure ranges they are able to achieve, with some consideration being given to the cost and availability of the material in the thicknesses needed. The 0.008-in. 6061-O, 0.032-in. 3303-H14, and the 0.025-in. 5052-H32 are the three materials which seem to most adequately cover the range of needed pressures. These materials have average differential bursting pressures of 31, 52, and 74 psi respectively. Combined, they actually permitted driver pressures of 35–150 psia, with a small gap near 65 psia.

In the future, in order to reach pressures higher than 150 psia, a material will need to be found that has a differential burst pressure much higher than the 74 psi reached by the 5052-H32 material. Also, an acetate film will be tested in order to find out if pressures lower than 35 psia can be reached (cp. Ref. [29]).

Maximum Temperature of Electroformed Nickel

The throat section of the Mach-6 quiet nozzle is electroformed onto a highly polished mandrel, using nearly pure nickel (see pp. 10-13 of Ref. [20]). Two different baths are used by GAR Electroforming, Danbury CT, in order to obtain a normal or "soft" nickel (nominally Rc 21-23) and a hard nickel (nominally Rc 33-38). The harder nickel interior is important to improve polishability and reduce the risk of developing scratches in the mirror finish.

Since the throat of the nozzle will be heated during operation, and since the nickel hardness can change due to annealing, tests were carried out to determine the nickel hardness both before and after it is heated to various temperatures. During normal operation, the nickel may reach driver-tube stagnation temperatures between 380K and 470K. According to Ref. [23], 380K is sufficient to avoid liquefaction, while 470K is the maximum tunnel temperature, well above the static-liquefaction requirement. In addition to this stagnation-temperature requirement, the throat region is fitted with a band heater that allows reaching higher temperatures, for control of nozzle wall instabilities [17, 18]. The maximum throat temperature will be limited by the properties of the electroformed nickel throat.

Various samples of the hard and soft nickel were obtained from GAR and used for the tests described on pp. 10-13 of Ref. [20]. Two of these nickel pieces, one of hard nickel and the other of soft nickel, were placed in an electric oven. The oven was then heated to approximately $200°F$, and the temperature was maintained for 48 to 72 hours. The nickel pieces were then removed and left to cool. Once cool, the pieces were tested using a Mitotoyo digital hardness tester, code no. 940-142. The Rockwell C-scale hardness was obtained at three different points on each piece, and the average of these was plotted versus the temperature. This process was then repeated at a slightly higher temperature, for a total of 13 different temperatures, including the initial run at room temperature.

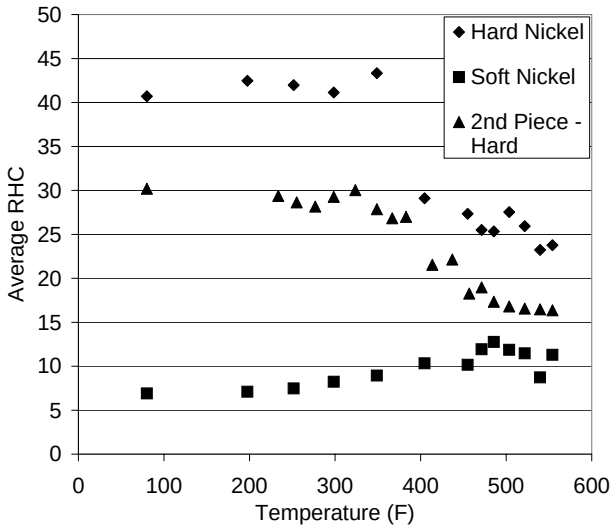

Figure 15: Hardness vs. Temperature for Electroformed Nickel

Figure 15 plots the hardness on the Rockwell C scale vs. the maximum temperature to which the part was heated. The soft nickel specimen is much softer than the nominal specification, while the two hard nickel specimens measure near the specification. A sudden drop in the hardness of the first hard nickel specimen was observed between $350°F$ (450K) and $405°F$ (480K). Since this is low enough to significantly limit the allowable throat-region overheat, a second hard nickel specimen was tested in the same manner, except that the hardness of the piece was tested at smaller temperature increments to improve resolution. The temperature at which the hardness drops repeats fairly well, and is resolved to be about $385°F$ (470K).

It thus seems that the throat temperature should be held below about 450K. If a stagnation temperature of 380K is sufficient to avoid liquefaction, as in Ref. [23], then it should be possible to raise the throat temperature about 50-100K above the stagnation temperature without damage. The

more conservative 50K limit will severely limit the possibilities for controlling nozzle-wall instabilities.

Electroformed Throat

The throat section of the nozzle is electroformed on a precision mandrel, as described on pp. 10-17 of Ref. [20] and pp. 4-5 of Ref. [21]. The mandrel was placed in the tank at GAR Electroforming at the end of June 2000, and the process was complete by the middle of September. It was carried out in two stages; halfway through, the electroform was removed and shipped to DEI so that the nodules that form on the outside surface could be machined down. A pin was used to fix the electroform so that it would not rotate during this process, and the high parts of the nodules were first cut off with a grinding wheel. The inner surface of the electroform is hard nickel, approx. 1/8-inch thick, with the outer portion of soft nickel.

After completion of the electroforming, the part was machined at DEI to form the outside of the bleed lip and to remove the overhang. The mandrel was then disassembled and pressed out. At this point, DEI expected to see a shiny polished electroform, and was discouraged to see black deposits interspersed on the shiny surface. These are believed to have come from the coolant and cutting fluid used in the machining processes. Apparently a very small gap opened up during the processing, perhaps from differential thermal expansion, and the fluids migrated in from capillary action. The electroform was shipped to Purdue for cleaning. Following the suggestion of Paul Thomas at Optical Technologies, Franklin Park, Illinois, the electroform was cleaned and polished with Happich Simichrome polish and clean cotton balls.

This process was successful in removing most of the contamination. A small parting line remained at the throat, along with some surface marks in the downstream region and near the throat, and some fine circumferential scratches near the exit. A skilled machinist estimated the parting line height as being less than 0.001 inches; it was present only around a portion of the circumference. The part was then shipped to Optical Technologies for a final polish.

Optical Technologies used a wood backing and a very fine diamond compound to remove the parting line and put a final polish on the throat region. They believe they were successful in removing the line without removing excess material. Contour measurements may be performed at DEI to verify the final throat contour, if these can be obtained with minimal risk of damaging the highly polished throat. Optical Technologies was also successful in removing the surface marks, which they believed to be mainly discolorations.

Bleed-Slot Vacuum System

The bleed-slot vacuum lines connect eight 1-inch openings in the nozzle throat assembly (pp. 15-17 of Ref. [19]) to the two 2-inch openings in the diffuser (pp. 8-9 of Ref. [21]). The lines are at full stagnation pressure before burst-diaphragm break (up to 300 psig), and then drop to vacuum pressure as the tunnel starts up. Since both the nozzle throat and the diffuser are allowed to roll streamwise when the nozzle or contraction are opened for cleaning or model insertion, 10-ft. flexible teflon-lined stainless-steel hoses are used to connect each section to fixed stainless piping. Stainless steel valves are located near the diffuser, to allow closing the bleed-slot suction lines. This enables comparisons under noisy-tunnel conditions, as in earlier work at NASA Langley.

A stainless-steel manifold was assembled at the throat to connect the eight 1-inch openings to a pair of 2-inch fittings for the hoses. Sanitary fittings are used to connect assemblies of welded fittings. Considerable care and rework were needed to achieve bubble-tight seals in the as-welded condition, due to distortions that occurred even during extremely careful welding. All welds were carefully performed with interior purge gas to avoid slag formation, and the assembly was carefully cleaned. Air was blown through the assembly into clean cloths, which were then checked under a microscope to ensure the assemblies are free of particles.

Hot-Wire Calibrations

Hot wires will be used to measure the mean flow and fluctuations in the boundary layer of future wind-tunnel models. Hot-wire technique is the only known method capable of measuring the very weak high-frequency instability waves with localized resolution [30]. It is also the least complex method capable of obtaining accurate mean-flow profiles in boundary layers with thicknesses of 0.010–0.080 inches. Pitot-probe methods generally suffer from probe interference [27, 31]. However, development of accurate hypersonic hot-wire calibrations is not trivial.

To ease the development of reliable calibrations, a 1-inch Mach-4 open-jet calibration tunnel was completed in summer 1999 [32, 33]. The facility

runs continuously from 1 atm. of stagnation pressure, eliminating unsteady effects, and allows independent variation of total pressure and total temperature. Hot wires have been installed and have survived 7 hours of continuous running. However, the pressure fluctuation level is about 10%. This is to be reduced to roughly 1% by installation of an improved settling chamber and contraction.

Calibrations also continue in the Mach-4 Ludwieg tube. In this facility, the stagnation temperature and pressure decrease slowly during the 3-4 s. runtime. Past attempts at calibration in this facility have uncovered problems with repeating the Nusselt-Reynolds curve [34, 35]. The problem occurs when measurements are carried out at nominally identical instantaneous conditions that are obtained during different portions of runs carried out from different initial conditions.

The hot wires used for the measurements presented here are welded using 90% Pt- 10% Rh wire with a diameter of 0.0001 in. The wire length is about 0.020–0.030 inches, and the wires are operated using the 1:1 bridge of a TSI IFA100 constant-temperature anemometer. The wire supports were adapted from those used earlier at the Jet Propulsion Laboratory (James Kendall, private communications, 1992-2000).

It has been discovered that one of the reasons for the past difficulty in matching Nusselt-Reynolds number curves is because the hot wire response was not repeatable. In order to obtain repeatable results, it is important to properly anneal and strain-harden the wire. If the hot wires are operated at a wire temperature higher than those previously used, the wire undergoes a new strain hardening which causes an increase in the room-temperature wire resistance. However, if the wire is operated at temperatures lower than those used in a previous strain hardening, the wire resistance, measured at room temperature, stays relatively constant.

These precautions seem consistent with those observed by previous investigators such as Dewey [36], Laufer and McClellan [37] and Smits et. al [38]. Dewey states that the largest changes in wire resistance occurred when the temperature or pressure of wire operation exceeded previous maxima. Laufer and McClellan also note that during the first several measurements for a given wire condition or overheat, the wire stretched permanently, due to the wind tunnel starting loads, which increased the wire resistance by 'several percent'. Dewey found that the wire resistance tended to increase between 2 and 8 percent with prolonged use. This trend has also been observed in the Mach-4 Ludwieg tube, for a wire that survived more than fifty runs. Dewey attributed this resistance increase to: (1) deformation phenomena (strain hardening), and (2) creep. Dewey controlled (1) by strain-hardening the wires at a maximum temperature and pressure that was not thereafter exceeded. Dewey also notes that the resistance variation could be minimized by 'heating the wire to a dull glow for several minutes prior to tunnel use' [36], which presumably has an annealing effect. Dewey notes that the creep effect was 'negligible after the first few hours of tunnel exposure'. Laufer and McClellan also used the 90% Pt-10% Rh wires; their smallest wire diameter was 0.00015 inches. They controlled repeatability by measuring the wire resistance both before and after a data set. If the resistance of the wire had changed by more than a few tenths of one percent, they discarded the results [37].

The measurements reported here were obtained after carefully following a new procedure. However, complete repeatability has not yet been obtained. So far, results are repeatable within individual sets of data for particular overheats. However, some drift in the wire resistance has been detected when changing the overheat, even after increasing to a maximum overheat and strain-hardening at that wire temperature. Procedural improvements are still being developed, therefore. The steps listed here lead to consistent results for a single wire overheat. However, in order to obtain massflow and temperature fluctuation data from the voltage fluctuations, data taken at a minimum of three different overheats will be required [39, 37, 40].

The following steps are presently being followed to obtain repeatable results:

1. The hot wire anemometer should be tuned and running for at least one hour prior to running the Ludwieg Tube.

2. Before the first run of a data set, the driver tube should be evacuated.

3. The wire must be strain-hardened at an temperature at least 70 K higher than the maximum overheat that is planned for the calibration. This should assure that additional strain-hardening will not occur during the calibration. However, this has still not been proven in our facility.

The first set of data, shown in Figure 16, was taken for a wire temperature of 600 K and a cold wire resistance, measured before and after the set

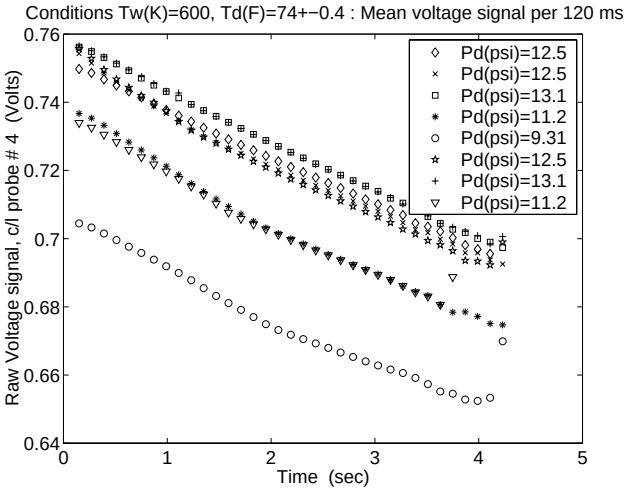

Figure 16: Raw voltage signal for a wire temperature of $T_w = 600$ K, averaged over 120 ms intervals.

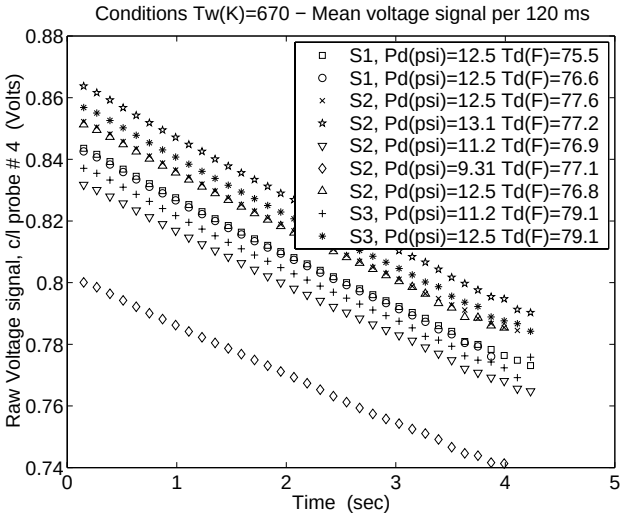

Figure 17: Averaged raw voltage signal for a wire temperature of $T_w = 670$ K.

of data, of 20.5±0.04 ohms. A straight freestream-type probe was used, and positioned so that the hotwire was at z = 11.3 inches from the throat (for details, see Refs. [35] or [41]). The flow in the Ludwieg tube is nearly steady for 120 ms periods between reflections of the expansion-wave in the driver tube; the data points shown here are averaged over these 120 ms periods. The initial driver tube pressure was set between 13.1000 psi and 9.3000 psi ± 0.0002 psi. The driver temperature was maintained at 74.0 ±0.4 ^{o}F by operating at night when natural variations were small. The conditions are listed in the order in which the runs were taken. There is a larger deviation between the first and second runs shown in Fig. 16, both taken at a driver pressure of 12.5 psi; this may be a result of the wire strain-hardening slightly. However, after the second run, the raw voltage is repeatable to 0.1%, for the given overheat.

An attempt was then made to increase the wire temperature. The room-temperature resistance also increased, in response to the additional strain-hardening. Data sets S1, S2, and S3 in Figure 17 were all obtained with the same overheat. Within set S1, the hotwire temperature was approximately 670 K and the room-temperature wire resistance changed from 20.52 ohms to 21.30 ohms ±0.05 ohms. The initial driver tube pressure was again varied between 13.1000 psi and 9.3000 psi ± 0.0002 psi.

The first run of each set has been disregarded, as it does not repeat well, possibly due to residual humidity that may accumulate in the driver tube overnight, or to wire strain-hardening effects. There was some difficulty re-tuning the wire between sets 1 and 2; a large adjustment was required, probably because of the nearly 1-ohm change in room-temperature wire resistance (about 5%). A drift is observed between sets 1 and 2. The drift between set 2 and 3 is not as large, however. This is despite the fact that the wire temperature was changed back to 600 K and then to 670 K between sets 2 and 3.

The error between sets 2 and 3 is about 1%, and the error within a set is less than 0.1%, with this 0.1% occuring for set 1 where the wire may still be strain hardening. There are some possible reasons for the voltage drift between the last two sets. The room-temperature wire resistance did change by 0.1 ohm (an increase of about 0.5%). The wire resistance continued to increase slightly; however, the resistance remained within 0.2 ohms of the value measured at the end of set 1. This increase may be due to Dewey's creep effect. Another possibility is that when the balance resistor was changed to obtain $T_w = 600$ K and then back to $T_w = 670$ K, the limiting overheat was insufficient, and the wire again strain-hardened. For future work, the wire will therefore be be strain hardened at a temperature at least 30-70 K higher than the highest overheat required for the experiment. Dewey's annealing process will also be attempted.

Finally, an overheat much less than the two cases already presented was chosen in order to validate the hypothesis that the wire would be repeatable when operated at decreased overheats. The wire temperature chosen was 530 K. As can be seen

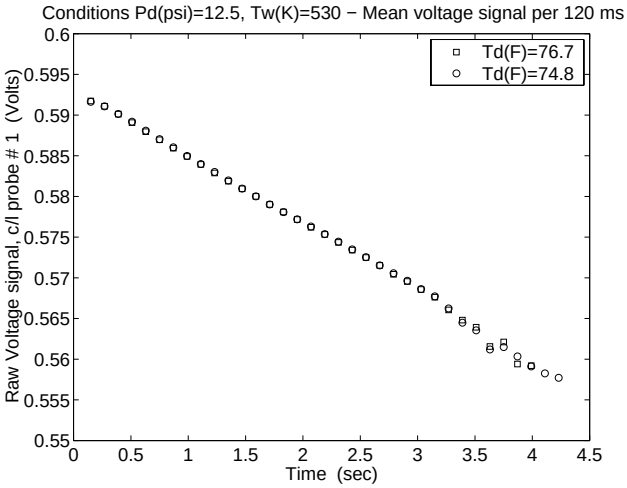

Figure 18: Averaged raw voltage signal for a wire temperature of $T_w = 530$ K.

in Figure 18, the results show remarkable repeatability, with an deviation of less than 0.02%. Here, the tunnel was evacuated before each run, and the two runs were obtained on different days, although the anemometer was not turned off between days. Unfortunately, the wire broke at this point, so that additional comparisons cannot be obtained.

These preliminary results show that close attention to the wire properties can enable obtaining repeatable results. However, further improvements remain necessary, and accurate calibrations must still be carried out. These should be possible, by combining the Mach-4 Ludwieg tube calibrations with the calibrations in the small open-jet tunnel. These calibrated wires and methods are then to be applied in the new Mach-6 Ludwieg tube, using the Mach-number independence principle.

Summary

The electroform for the nozzle throat has been successfully fabricated. A final direct polishing was necessary to remove the parting line. The first two downstream nozzle sections have also been completed successfully. Delivery of the last nozzle sections is presently scheduled for February 2001.

Computations of the temperature distribution in the nozzle show that free convection will bring the nozzle near to room temperature less than halfway from the throat to the downstream end. Computations of the nozzle-wall instability using these temperature distributions indicate that transition on the nozzle wall will occur earlier than desirable. If experience bears out this early transition, the wall-temperature distribution will have to be tailored to delay the nozzle wall transition.

The burst diaphragm apparatus has been completed, and diaphragm materials have been identified and tested for operation between 35 and 150 psia. Improved techniques for operation and calibration of hot wires have also been developed. Careful attention to wire annealing and strain-hardening is necessary to achieve repeatable results.

Acknowledgements

The research is funded by AFOSR under grant F49620-00-1-0016, monitored by Steve Walker, and by Sandia National Laboratory, under contract BG-7114. Fabrication of the tunnel was supported primarily by a gift from the Boeing Company and two grants from the Defense University Research Instrumentation Program (F49620-98-1-0284 and F49620-99-1-0278). The first grant was funded by AFOSR, and the second was funded jointly by AFOSR and BMDO. Tunnel fabrication has also been supported by Sandia National Laboratory, and by a gift in memory of K.H. Hobbie.

The tunnel design and fabrication has been carried out in cooperation with Dynamic Engineering Inc., of Newport News, Virginia. The fabrication specifications are often extremely tight, and DEI's program manager, Larry DeMeno, has made an excellent effort toward meeting them. Paul Thomas of Optical Technologies, Franklin Park, Illinois, has been very helpful in developing methods for polishing the critical throat-region mandrel and electroform. The generous cooperation of Dr. Steve Wilkinson and the rest of the NASA Langley quiet tunnel group has also been critical to our progress. The digital hardness tester was made available by Purdue Aviation Technology, courtesy of Prof. W. Watkins. Mr. Mike Rapp designed the bleed-slot vacuum lines.

References

[1] Scott A. Berry, Thomas J. Horvath, Brian R. Hollis, Richard A. Thompson, and H. Harris Hamilton II. X-33 hypersonic boundary layer transition. Paper 99-3560, AIAA, June 1999.

[2] H.A. Korejwo and M.S. Holden. Ground test facilities for aerothermal and aero-optical evaluation of hypersonic interceptors. Paper 92-1074, AIAA, February 1992.

[3] AGARD. *Sustained Hypersonic Flight*, April 1997. CP-600, vol. 3.

[4] Tony C. Lin, Wallis R. Grabowsky, and Kevin E. Yelmgren. The search for optimum configurations for re-entry vehicles. *J. of Spacecraft and Rockets*, 21(2):142–149, March-April 1984.

[5] I.E. Beckwith and C.G. Miller III. Aerothermodynamics and transition in high-speed wind tunnels at NASA Langley. *Annual Review of Fluid Mechanics*, 22:419–439, 1990.

[6] Steven P. Schneider. Effects of high-speed tunnel noise on laminar-turbulent transition. Paper 2000-2205, AIAA, June 2000. Revised version to appear in the J. Spacecraft and Rockets.

[7] Steven P. Schneider. Flight data for boundary-layer transition at hypersonic and supersonic speeds. *Journal of Spacecraft and Rockets*, 36(1):8–20, 1999.

[8] F.-J. Chen, M.R. Malik, and I.E. Beckwith. Boundary-layer transition on a cone and flat plate at Mach 3.5. *AIAA Journal*, 27(6):687–693, 1989.

[9] S. P. Wilkinson, S. G. Anders, and F.-J. Chen. Status of Langley quiet flow facility developments. Paper 94-2498, AIAA, June 1994.

[10] I. Beckwith, T. Creel, F. Chen, and J. Kendall. Freestream noise and transition measurements on a cone in a Mach-3.5 pilot low-disturbance tunnel. Technical Paper 2180, NASA, 1983.

[11] Alan E. Blanchard, Jason T. Lachowicz, and Stephen P. Wilkinson. NASA Langley Mach 6 quiet wind-tunnel performance. *AIAA Journal*, 35(1):23–28, January 1997.

[12] S. P. Schneider and C. E. Haven. Quiet-flow Ludwieg tube for high-speed transition research. *AIAA Journal*, 33(4):688–693, April 1995.

[13] Steven P. Schneider, Steven H. Collicott, J.D. Schmisseur, Dale Ladoon, Laura A. Randall, Scott E. Munro, and T.R. Salyer. Laminar-turbulent transition research in the Purdue Mach-4 quiet-flow Ludwieg tube. Paper 96-2191, AIAA, June 1996.

[14] J.D. Schmisseur, Steven H. Collicott, and Steven P. Schneider. Laser-generated localized freestream perturbations in supersonic and hypersonic flows. *AIAA Journal*, 38(4):666–671, April 2000.

[15] Terry R. Salyer, Steven H. Collicott, and Steven P. Schneider. Feedback stabilized laser differential interferometry for supersonic blunt body receptivity experiments. Paper 2000-0416, AIAA, January 2000.

[16] Dale W. Ladoon and Steven P. Schneider. Measurements of controlled wave packets at Mach 4 on a cone at angle of attack. Paper 98-0436, AIAA, January 1998.

[17] Steven P. Schneider. Design of a Mach-6 quiet-flow wind-tunnel nozzle using the e**N method for transition estimation. Paper 98-0547, AIAA, January 1998.

[18] Steven P. Schneider. Laminar-flow design for a Mach-6 quiet-flow wind tunnel nozzle. *Current Science*, 79(6):790–799, 25 September 2000.

[19] Steven P. Schneider. Design and fabrication of a 9-inch Mach-6 quiet-flow Ludwieg tube. Paper 98-2511, AIAA, June 1998.

[20] Steven P. Schneider. Fabrication and testing of the Purdue Mach-6 quiet-flow Ludwieg tube. Paper 2000-0295, AIAA, January 2000.

[21] Steven P. Schneider. Initial shakedown of the Purdue Mach-6 quiet-flow Ludwieg tube. Paper 2000-2592, AIAA, June 2000.

[22] Steven P. Schneider, Craig Skoch, and Shann Rufer. Mean flow and noise measurements in the Purdue Mach-6 quiet-flow Ludwieg tube. Paper 2001-XXXX, AIAA, June 2001. Submitted to the June 2001 AIAA Fluid Dynamics Meeting.

[23] D.A. Bountin, A.N. Shiplyuk, and A.A. Sidorenko. Experimental investigations of disturbance development in the hypersonic boundary layer on a conical models. In H. Fasel and W. Saric, editors, *Laminar-Turbulent Transition. Proceedings of the IUTAM Symposium, Sedona, 1999*, Berlin, 2000. Springer-Verlag. To appear.

[24] C.J. Schueler. An investigation of model blockage for wind tunnels at Mach numbers 1.5 to 19.5. Technical Report AEDC-TN-59-165, Arnold Engineering Development Center, February 1960. DTIC citation AD-232492. Limited distribution.

[25] Frank P. Incropera and David P. Dewitt. *Introduction to Heat Transfer*. John Wiley and Sons, New York, 3rd edition, 1996.

[26] Klaus Hannemann. Numerical flow field analyses of the RWG Mach 6.8 contoured nozzle. Technical Report IB 223-95 A 46, Deutsche Forschungsanstalt für Luft- und Raumfahrt, Göttingen, Germany, May 1996. In English.

[27] James M. Kendall, Jr. An experimental investigation of leading-edge shock-wave–boundary-layer interaction at Mach 5.8. *J. Aero. Sci.*, 24:47–56, January 1957.

[28] Shann J. Rufer. Development of burst-diaphragm and hot-wire apparatus for use in the Mach-6 Purdue quiet-flow Ludwieg tube. Master's thesis, School of Aeronautics and Astronautics, Purdue University, December 2000.

[29] H. Knauss, R. Riedel, and S. Wagner. The shock wind tunnel of Stuttgart university: a facility for testing hypersonic vehicles. Paper 99-4959, AIAA, November 1999.

[30] S.H. Collicott, S.P. Schneider, and N.L. Messersmith. Review of optical diagnostics for hypersonic low-noise Ludwieg tube facilities. Paper 96-0851, AIAA, January 1996.

[31] M. V. Morkovin and W.S. Bradfield. Probe interference in measurements in supersonic laminar boundary layers. *Journal of the Aeronautical Sciences*, 21(11):785–787, November 1954.

[32] Phillip M. Schneider. Flow measurements in a Mach 4 axisymmetric jet. Purdue University, School of Aeronautics and Astronautics. A 29 page laboratory report with 11 figures, May 1999.

[33] Phillip M. Schneider. Design and construction of a Mach 6 hot wire calibration jet. Purdue University, School of Aeronautics and Astronautics. A 30 page laboratory report, plus extensive appendices, December 1998.

[34] Dale W. Ladoon. *Wave packets generated by a surface glow discharge on a cone at Mach 4.* PhD thesis, School of Aeronautics and Astronautics, Purdue University, December 1998.

[35] J. D. Schmisseur. *Receptivity of the Boundary Layer on a Mach-4 Elliptic Cone to Laser-Generated Localized Freestream Perturbations.* PhD thesis, School of Aeronautics and Astronautics, Purdue University, December 1997.

[36] C. Forbes Dewey, Jr. Hot wire measurements in low Reynolds number hypersonic flows. *ARS Journal*, pages 1709–1718, December 1961.

[37] John Laufer and Robert McClellan. Measurements of heat transfer from fine wires in supersonic flows. *Journal of Fluid Mechanics*, 1:276–289, 1956. Part 1.

[38] A. J. Smits, K. Hayakawa, and K. C. Muck. Constant temperature hot-wire anemometer practice in supersonic flows. *Experiments in Fluids*, 1:83–92, 1983. Part 1: The Normal Wire.

[39] Leslie S. G. Kovasznay. The hot-wire anemometer in supersonic flow. *Journal of the Aeronautical Sciences*, pages 565–584, September 1950.

[40] C. L. Ko, D. K. McLaughlin, and T. R. Troutt. Supersonic hot-wire fluctuation data analysis with a conduction end-loss correction. *Journal of Physics E: Scientific Instruments*, 11:488–492, 1978.

[41] Steven P. Schneider, Christine E. Haven, Joseph B. McGuire, Steven H. Collicott, Dale Ladoon, and Laura A. Randall. High-speed laminar-turbulent transition research in the Purdue quiet-flow Ludwieg tube. Paper 94-2504, AIAA, June 1994.